

A&A manuscript no.

(will be inserted by hand later)

Your thesaurus codes are:

06(08.14.1; 08.05.3; 02.04.1; 02.13.1; 13.25.5)

ASTRONOMY
AND
ASTROPHYSICS

Neutron superfluidity in strongly magnetic interiors of neutron stars and its effect on thermal evolution

Ch. Schaab*, F. Weber, and M. K. Weigel

Institut für theoretische Physik, Ludwig-Maximilians Universität München, Theresienstr. 37, D-80333 München, Germany

Received: October 6, 1997 / Accepted March 31, 1998

Abstract. The possibility of a neutron $m = 2$ -superfluid in the interior of neutron stars is investigated. This pairing state is energetically favoured in strong magnetic fields ($H \sim 10^{16} - 10^{17}$ G). Because of the node in the angular-dependent energy gap along the field direction the neutrino emissivity is only suppressed polynomially as function in T/T_c instead of exponentially, as it is obtained for a nodeless pairing state. The effect of this pairing state on the thermal evolution of neutron stars is studied, and its outcome is compared with the evolution of “normal”, i.e. nodeless, superfluid and non-superfluid neutron stars, and also with observations. We find that particularly the predicted surface temperatures of the enhanced cooling scenario considerably change and come into agreement with temperatures deduced from observational data within the hydrogen atmosphere model. Furthermore the surface temperature depends on the magnetic field strength as an additional parameter aside from the neutron star mass. The latter is however only operative in the case of the intermediate cooling scenario.

Key words: Stars: neutron – Stars: evolution – Dense matter – Magnetic fields – X-rays: stars

1. Introduction

Comparison of soft X-ray and extreme UV observations with simulations of the thermal evolution of neutron stars gives us a powerful tool for investigating the interior of such stars, since young neutron stars cool mainly via neutrino emission from there. The rate of neutrino emission depends on a number of ingredients, among which the composition and the superfluid pairing play the most important roles.

Differences in the composition of various models make it sensible to distinguish between slow (or standard) and enhanced scenarios of thermal evolution, depending on whether the dominant process is either the modified or the direct Urca. As it was shown in Schaab et al. (1997)

(see also Voskresenskii & Senatorov, 1986) the uncertainties in the degree of modifications of the modified Urca rate by medium effects suggest a third possible scenario, the intermediate cooling scenario.

It is generally believed that neutrons in the interior of a neutron star form superfluid pairs in a 3P_2 -state below some critical temperature $T_c \sim 10^9$ K. Since this high density ($\rho > \rho_0 = 2.8 \times 10^{14}$ g cm $^{-3}$) matter in β -equilibrium is not directly accessible by laboratory experiments, one can only extrapolate the two-body interaction to this regime. The pairing gaps however depend very sensitively on the underlying microscopic model for the effective nucleon–nucleon interaction. Its value and the density range over which pairing occurs is therefore quite uncertain. Another uncertainty concerning the 3P_2 -pairing of neutrons refers to the angular dependency of the gap. In isotropic matter the $m = 0$ -angular dependency $\Delta^2(\mathbf{k}) \propto 1/3 + \cos^2 \theta$ is energetically favoured (Hoffberg et al., 1970). Above some critical magnetic field strength $H_c \sim 10^{16} - 10^{17}$ G however the free energy is minimised by a $m = 2$ -dependency $\Delta^2(\mathbf{k}) \propto \sin^2 \theta$, where θ is the angle between the quasiparticle momentum \mathbf{k} and the magnetic field direction (Muzikar et al., 1980). This different angular dependency turns out to be important for the cooling behaviour of superfluid neutron stars, since the $m = 2$ -angular dependency has nodes at $\theta = 0, \pi$. The available phase space of the various processes keeps therefore undiminished in the direction of the magnetic axis, and the reaction rates are only suppressed polynomially instead of exponentially (Anderson & Morel, 1961; Levenfish & Yakovlev, 1994b).

The observed surface magnetic fields of neutron stars ranges from $B = 1.7 \times 10^8$ G (PSR B1957+20) up to 2.1×10^{13} G (PSR B0154+61), with a median value of about 10^{12} G. These values are deduced from the observed spin-down velocity of 558 pulsars by assuming the magnetic dipole braking model (see the pulsar catalog by Taylor et al., 1993)). Because of the highly conducting core the surface may hide an even stronger magnetic field in the interior (Muslimov & Page, 1996). By applying the Newtonian scalar virial theorem Lai & Shapiro (1991) showed that the interior field may be as high as 10^{18} G. Works on

* E-mail address: schaab@gsm.sue.physik.uni-muenchen.de

the origin and evolution of the interior magnetic field show that at least field strengths of $H = 10^{15}$ to 10^{17} G are possible (Bisnovatyi-Kogan & Moschenko, 1992; Bisnovatyi-Kogan, 1993; Duncan & Thompson, 1992; Thompson & Duncan, 1993), which is in the range of the critical field strength for $m = 2$ -superfluidity.

Besides the neutrons also the protons supposedly pair in the interior of a neutron star. Since they probably form a type II-superconductor, the magnetic field is confined to flux tubes, whose radial dimension is given by the London penetration depth, $\lambda \sim 40\text{--}100$ fm. The magnetic field inside the flux tubes is therefore of the order of $H \approx \Phi_0 \ln(\lambda/\xi)/2\pi\lambda^2 \sim 10^{14}\text{--}10^{16}$ G, where $\Phi_0 \approx 2.1 \times 10^{-7}$ G cm² is the flux quantum and $\xi \sim 10$ fm is the coherence length. Even if the bulk of the neutrons do not experience a field above the critical field H_c , the field inside the flux tubes may be large enough. This would be sufficient for a considerable modification of the thermal properties of a neutron star.

In this work we will study the effect of nodes of the neutron gap energy along the magnetic axis on the thermal evolution of neutron stars and compare the results with neutron star models with 3P_2 -pairing in the $m = 0$ -state and also with observed data. We will start with the underlying physics by discussing the energetically favoured pairing state in 3P_2 -superfluidity and the suppression of the most important neutrino emission processes (Sect. 2 and 3). In Sect. 4 we classify our models into 16 scenarios. The outcome of the simulations for these scenarios is compared with observations in Sect. 5. Section 6 contains the conclusions and the discussion.

2. 3P_2 -pairing

Neutrons are believed to form 1S_0 -superfluid pairs in the density range between neutron drip and the saturation density of normal nuclear matter. At supernuclear densities, i.e. in the core regime of neutron stars, the repulsive interaction becomes dominant and the 1S_0 -superfluidity gap closes. However, the tensor and spin-orbit interaction become attractive at such densities and the formation of 3P_2 -neutron pairs becomes possible. The ordering parameter for 3P_2 -pairing is a complex, traceless, symmetric 3x3-matrix \mathbf{A} . It can be determined in vicinity of the transition temperature T_c by minimising the Ginzburg-Landau free-energy functional $\Omega[\mathbf{A}]$. This was done by Muzikar et al. (1980), who found that for a magnetic field strength

$$H > H_c(T) = 3 \times 10^{17} \frac{k_B T_c}{1 \text{ MeV}} \left(1 - \frac{T}{T_c}\right) \text{ G} \quad (1)$$

the energy gap for quasiparticle of momentum \mathbf{p} is

$$|\Delta_{m=2}(\hat{p})|^2 = \frac{3}{8\pi} \Delta_{m=2}^2(T) \sin^2 \theta. \quad (2)$$

Here, k_B denotes the Boltzmann-constant, θ the angle between the magnetic field \mathbf{H} and quasiparticle momentum

\mathbf{p} , \hat{p} the unit vector in direction of \mathbf{p} , and $\Delta_{m=2}^2(T)$ a temperature dependent factor. For vanishing magnetic fields the free energy functional is minimised by the gap function

$$|\Delta_{m=0}(\hat{p})|^2 = \frac{1}{16\pi} \Delta_{m=0}^2(T) (1 + 3 \cos^2 \theta'), \quad (3)$$

where θ' is the angle between \mathbf{p} and some quantisation axis. As we have already noted the gap function (2) vanishes along the magnetic axis at $\theta = 0, \pi$, whereas the gap function (3) is nodeless. For magnetic fields $0 < H < H_c(T)$ the minimising gap function is a superposition of Eqs. 2 and 3, which is still nodeless.

The critical field strength vanishes at the critical temperature T_c and increases to

$$H_c(T = 0) = 3 \times 10^{17} \frac{k_B T_c}{1 \text{ MeV}} \text{ G} \quad (4)$$

at $T = 0$. In the pairing model of Hoffberg et al. (1970) the maximum energy gap is, for instance, $\Delta_{\max} \approx 4.5$ MeV. This yield a critical field strength $H_c(T = 0) \approx 2 \times 10^{17}$ G. If the inner magnetic field is smaller than $H_c(T = 0)$, first a $m = 2$ -superfluid is formed at T_c and then at

$$T_{c,2} = T_c \left(1 - \frac{H}{H_c(T = 0)}\right) \quad (5)$$

a nodeless $m = 0$ -superfluid is formed.

3. Neutrino emissivity in superfluid matter

In the vicinity of the Fermi surface ($|p - p_F| \ll p_F$) the one-particle energy can be approximated by (see, e.g., Lifshitz & Pitaevskii, 1980)

$$E(\mathbf{p}) = \mu \begin{cases} -\sqrt{|\Delta(\hat{p})|^2 + v_F^2(p - p_F)^2} & \text{for } p < p_F, \\ +\sqrt{|\Delta(\hat{p})|^2 + v_F^2(p - p_F)^2} & \text{for } p \geq p_F, \end{cases} \quad (6)$$

where v_F , p_F , and μ is the Fermi velocity, momentum, and energy, respectively. The superfluidity creates a gap of width $2|\Delta(\hat{p})|$ in the energy spectrum around the Fermi momentum p_F . Excitations of particles above the Fermi energy are therefore suppressed for $k_B T < |\Delta(\hat{p})|$. We shall study the two possible cases of triplet pairing of neutrons which occur (or might occur) in neutron stars' interior (see Sect. 2). The gap function $|\Delta_{m=0}(\hat{p})|$ in the case of nodeless pairing (Eq. 3) has the approximate form (Levenfish & Yakovlev, 1994b)

$$|\Delta(\hat{p})_{m=0}| = \sqrt{1 - \frac{T}{T_c}} \left(0.7893 + 1.188 \frac{T_c}{T}\right) k_B T \times \sqrt{1 + 3 \cos^2 \theta}, \quad (7)$$

whereas gap (2) gives

$$|\Delta(\hat{p})_{m=2}| = \sqrt{1 - \left(\frac{T}{T_c}\right)^4} \times \left(2.030 - 0.4903 \left(\frac{T}{T_c}\right)^4 + 0.1727 \left(\frac{T}{T_c}\right)^8\right) \frac{T_c}{T} k_B T \sin \theta. \quad (8)$$

The suppression of the neutrino emissivity ϵ_ν by superfluid neutrons can be expressed by a factor

$$\mathcal{R}_n = \frac{\epsilon_\nu^{\text{sf}}}{\epsilon_\nu^{\text{n,sf}}}, \quad (9)$$

which was calculated for a couple of processes in Levenfish & Yakovlev (1994b) and Yakovlev & Levenfish (1995). Let us consider for example the direct Urca process (Boguta, 1981; Lattimer et al., 1991)

$$n \rightarrow p + e^- + \bar{\nu}_e. \quad (10)$$

The suppression factor can analytically be calculated only in the limiting case $T \rightarrow 0$ (Levenfish & Yakovlev, 1994b)

$$\mathcal{R}_n^d = \begin{cases} \frac{126}{457\pi^5} \sqrt{\frac{1}{3}v^5 e^{-v}} & \text{for case } m = 0, \\ \frac{6029\pi^2}{5484} v^{-2} & \text{for case } m = 2, \end{cases} \quad (11)$$

where the dimensionless parameter v is given by

$$v = \begin{cases} \sqrt{\frac{1}{16\pi} \frac{\Delta(T)}{k_B T}} & \text{for case } m = 0, \\ \sqrt{\frac{3}{8\pi} \frac{\Delta(T)}{k_B T}} & \text{for case } m = 2. \end{cases} \quad (12)$$

By numerical fitting Levenfish & Yakovlev (1994b) obtain

$$\mathcal{R}_n^d = \begin{cases} \left(0.2546 + \sqrt{(0.7454)^2 + (0.1284v)^2}\right)^5 \\ \times \exp\left(2.701 - \sqrt{(2.701)^2 + v^2}\right) & \text{for } m = 0, \\ \frac{1}{2} + \frac{0.09226v^2}{1 + (0.1821v)^2 + (0.16736v)^4} \\ + \frac{1}{2} \exp\left(1 - \sqrt{1 + (0.4129v)^2}\right) & \text{for } m = 2. \end{cases} \quad (13)$$

As can be deduced from Eq. 11, the suppression factors of the nodeless case $m = 0$ decreases with decreasing temperature much more rapidly than the suppression factor for case $m = 2$ (see Fig. 1). This is caused by the two nodes of the gap function at the intersections of the Fermi surface with the magnetic axis.

Besides the direct Urca process we considered a couple of other processes (see Table 1). Following Levenfish & Yakovlev (1996) we approximate the suppression factors for these processes by

$$\mathcal{R}_n^1(v) = \mathcal{R}_n^d(v), \quad (14)$$

if only one neutron is involved (proton branch of modified Urca process, electron-neutron, and neutron-proton scattering), and by

$$\mathcal{R}_n^2(v) = \mathcal{R}_n^d(2v), \quad (15)$$

if two neutrons are involved (neutron branch of modified Urca process and neutron-neutron scattering).

The suppression factors for proton superconductivity are given in Yakovlev & Levenfish (1995). If both neutrons and proton are superfluid we approximate the combined suppression factor \mathcal{R}_{np} by the minimum of the factors \mathcal{R}_n

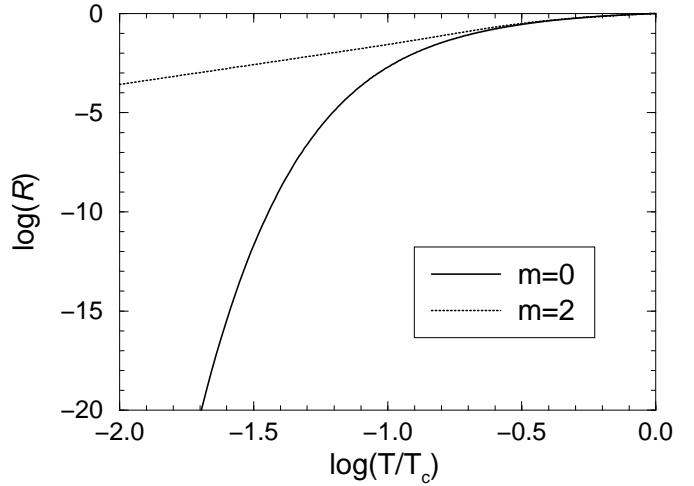


Fig. 1. Suppression factor \mathcal{R}_n^d of the direct Urca process for the two cases of triplet pairing.

and \mathcal{R}_p obtained by neglecting the superfluidity of the other nuclear species (cf. Levenfish & Yakovlev, 1996):

$$\mathcal{R}_{np} \approx \min(\mathcal{R}_n, \mathcal{R}_p). \quad (16)$$

We account also for the suppression of the heat capacity (Levenfish & Yakovlev, 1994a) and of the heat conductivity (Gnedin & Yakovlev, 1995). Thought the factors are similar as in the case of neutrino processes, the effect on the thermal history is only small compared to the effect of the suppression of the neutrino emissivity. In the case of the heat capacity at least electrons and possibly also non superfluid protons and hyperons still contribute to the total heat capacity, whereas the heat conductivity is maintained by electron-electron, electron-muon, and muon-muon scattering processes.

4. Cooling scenarios

The general relativistic equations of stellar structure and thermal evolution (cf. Thorne, 1977) were numerically solved via an implicit finite difference scheme by a Newton-Raphson algorithm (see Schaab et al., 1996 for more details). The outcome of the simulations depend on a couple of ingredients which are partly rather uncertain. If one took all these uncertainties into account, one would get a huge number of models, which are difficult to survey. However all these models can be divided into four distinct classes depending on the dominant neutrino process (Schaab et al., 1997). These are:

Class A – Standard cooling: This class consists of slowly cooling models which do not allow for any enhanced cooling process (like the direct Urca process).

Class B – Intermediate cooling: The emission rate of the modified Urca process is increased by medium effects (Voskresenskii & Senatorov, 1986; Schaab et al., 1997).

Table 1. Neutrino processes considered in the cooling simulations

Process	Emissivity from Ref.
pair-, photon-, plasma-processes	Itoh et al. (1989)
bremssstrahlung in the crust	Yakovlev & Kaminker (1996); Haensel et al. (1996)
bremssstrahlung in the core:	
n-n scattering	Friman & Maxwell (1979)
n-p scattering	Friman & Maxwell (1979)
p-p scattering	Friman & Maxwell (1979)
e ⁻ -n scattering	Kaminker et al. (1997)
e ⁻ -p scattering	Kaminker et al. (1997)
e ⁻ -F scattering	Kaminker et al. (1997)
superfluid pair breaking and formation	Voskresenski [†] & Senatorov (1987); Schaab et al. (1997); †
modified nucleon Urca:	
neutron branch	Friman & Maxwell (1979)
or alternatively	Voskresenski [†] & Senatorov (1986); Schaab et al. (1997)
proton branch	Yakovlev & Levenfish (1995)
direct nucleon Urca	Lattimer et al. (1991)
direct hyperon Urca	Prakash et al. (1992)

†: In the case of 3P_2 -pairing the emissivity was recalculated by averaging over the angle θ between quasiparticle momentum \mathbf{p} and quantisation axis (s. Eqs. 2, 3)

This leads to a considerably faster cooling during the neutrino cooling era.

Class C – Enhanced nucleon cooling: The third class allows for the direct nucleon Urca process (maybe in combination with pion or kaon condensation) yielding an even faster cooling than in the intermediate cooling scenario.

Class D – Enhanced hyperon cooling: The last class allows additionally or exclusively for the direct hyperon Urca process, which is not suppressed by nucleon superfluidity in contrast to the nucleon processes¹.

The possibility of the direct nucleon and hyperon Urca process depends on the composition in the interior of the star and hence on the underlying equation of state and on the central density of the star. The equations of state can therefore also be divided into these four classes, if the mass of the neutron star model is fixed to some value (we selected the canonical value $M = 1.4M_{\odot}$). Such a division is done in Table 2. We used a broad collection of equations of state which comprises relativistic field-theoretical models, one non-relativistic Thomas-Fermi model, as well as non-relativistic Schrödinger-based ones. The first two classes, the standard and the intermediate cooling classes, base on the same set of equations of state, but on different neutrino emission rates of the modified Urca process. The division in two different classes seems sensible, since the rate of this process depends quite sensitively on the choice of the microscopic parameters – as, for instance,

¹ The ability of hyperons to form superfluid or superconducting pairs has only recently been investigated (Balberg & Barnea, 1998). We shall assume here that hyperons cannot pair and address this problem in a forthcoming work (Schaab et al., 1998).

the effective pion gap – which are unfortunately rather uncertain.

As already mentioned in Sect. 1 the second important uncertainty concerns the superfluidity of neutrons in the interior of the star. Again we classify the possible models into four classes:

Class 1: Neutrons pair in the nodeless 3P_2 -state ($m = 0$).
 Class 2: The inner, uniform magnetic field strength H exceeds its critical value $H_c(T = 0) \approx 2 \times 10^{17}$ G (see Eq. 1) even for zero temperature. The neutrons therefore form a $m = 2$ -superfluid.

Class 3: The inner magnetic field is set to $H = 10^{17}$ G < H_c . The critical field strength is therefore exceeded for temperatures $T_{c,2} \leq T \leq T_c$ only.

Class 4: Either the critical temperature of neutron pairing is very small (e.g. Elgarøy et al., 1996a), or the superfluid phase does not extend over the whole interior of the neutron star (e.g. Takatsuka, 1972).

For the classes 1–3 we used the gap energy by Hoffberg et al. (1970)². For class 4 we used the models by Elgarøy et al. (1996a) and Takatsuka (1972). The angle-averaged energy gaps of 3P_2 -pairing in the $m = 0$ - and $m = 2$ -states are almost equal (Elgarøy et al., 1996b). We can therefore approximate the energy gap for the $m = 2$ -state, which is not given by all authors, by $\Delta_{m=2}(T) \approx \sqrt{\frac{1}{2}}\Delta_{m=0}$ (Amundsen & Østgaard, 1985).

² Hoffberg et al. (1970) estimated the gap energy of 3P_2 -pairing by using the phase shift data of neutron–neutron scattering and assuming the effective nucleon mass to be equal to its bare mass. The obtained gap energy serves therefore as an upper limit and is used here to demonstrate the effect of $m = 2$ -pairing.

Table 2. Classification of equations of state into the four cooling classes defined in the text. The canonical neutron star mass $M = 1.4M_{\odot}$ is assumed. The classification into the standard and intermediate cooling class depends on whether or not medium modification of the modified Urca process are taken into account.

Class	EOS	Baryonic composition	Interaction	Many-body approach	Ref.
A/B	UV ₁₄ +UVII	p,n	2 nuclei potential Urbana V ₁₄ and 3 nuclei potential Urbana VII	NRV	1
A/B	UV ₁₄ +TNI	p,n	2 nuclei potential Urbana V ₁₄ and density dependent terms TNI	NRV	1
A/B	TF	p,n	2 nuclei potential TF	NRTF	2
C	HV _{pn}	p,n	exchange of σ, ω, ρ mesons	RH	3
C	RHF _{pn}	p,n	exchange of $\sigma, \omega, \rho, \pi$ mesons	RHF	4
C	G _{pn} ^{K240}	p,n	exchange of σ, ω, ρ mesons	RH	5
D	HV	p,n,Λ,Σ ^{±,0} ,Ξ ^{0,-}	exchange of σ, ω, ρ mesons	RH	3
D	RHF1	p,n,Λ,Σ ^{±,0} ,Ξ ^{0,-} ,Δ	exchange of $\sigma, \omega, \rho, \pi$ mesons	RHF	4
D	RHF8	p,n,Λ,Σ ^{±,0} ,Ξ ^{0,-} ,Δ	exchange of $\sigma, \omega, \rho, \pi$ mesons	RHF	4
D	G _{M78} ^{K240}	p,n,Λ,Σ ^{±,0} ,Ξ ^{0,-}	exchange of σ, ω, ρ mesons	RH	5
D	G _{M78u} ^{K240}	p,n,Λ,Σ ^{±,0} ,Ξ ^{0,-}	exchange of σ, ω, ρ mesons	RH	5

Abbreviations: NRV: non-relativistic variational method, NRTF: non-relativistic Thomas-Fermi model, RH: relativistic Hartree approximation, RHF: relativistic Hartree-Fock approximation. References: 1: Wiringa et al. (1988), 2: Strobel et al. (1997), 3: Weber & Weigel (1989), 4: Huber et al. (1997), 5: Glendenning, priv. comm.

The cooling simulations are performed by running the numerical code for all combinations of parameters which are in agreement with the respective cooling scenario (a detailed list of all parameters can be found on the Web: <http://www.physik.uni-muenchen.de/sektion/suessmann/astro/cool/schaab.0797/input.html>). This procedure leads to cooling bands rather than individual cooling tracks, by means of which we demonstrate the uncertainty inherent in the input parameters. By combining the four classes of equations of state A–D with the four classes of superfluidity 1–4 we get a collection of sixteen scenarios whose behaviour will be studied in the next section.

We shall study the case where the magnetic field exceeds $H_c(T = 0)$ only inside the flux tubes of the proton type II-superconductor separately. In this case (labeled as class 2γ), the suppression factor \mathcal{R} can be expressed by the combination

$$\mathcal{R} = \gamma \mathcal{R}_{\text{in}} + (1 - \gamma) \mathcal{R}_{\text{out}} \quad (17)$$

of the suppression factors \mathcal{R}_{in} , \mathcal{R}_{out} inside and outside the tubes. γ is the volume fraction occupied by the proton flux tubes. Inside the tubes we assume that the magnetic field exceeds the critical field strength $H_c(T = 0)$. Because protons are unpaired inside, the suppression factor \mathcal{R}_{in} is equal to the suppression factor for neutron $m = 2$ -pairing. Since the magnetic field is constrained to the flux tubes, neutron pair in a nodeless $m = 0$ -state outside the tubes. \mathcal{R}_{out} accounts for both superfluids, the nodeless neutron superfluid and the singlet proton superfluid by the approximate expression of Eq. (16). The volume fraction γ is determined by the relation

$$\gamma = \frac{H_{\text{ex}}}{H_{\text{tube}}} \quad (18)$$

of the bulk field strength H_{ex} and the field strength inside the proton flux tubes H_{tube} , which we set equal to the critical field strength $H_c(T = 0) \approx 2 \times 10^{17}$ G.

5. Results and comparison with observations

Among the soft X-ray observations of the 27 sources which were identified as pulsars, the ROSAT and ASCA observations of PSRs 0002+62, 0833-45 (Vela), 0656+14, 0630+18 (Geminga) and 1055-52 (see Table 3) achieved a sufficiently high photon flux such that the effective surface temperatures of these pulsars could be extracted by two- or three-component spectral fits (Ögelman, 1995). The obtained effective surface temperatures, shown in Figs. 2 to 6, depend crucially on whether a hydrogen atmosphere is used or not. The kind of atmosphere of individual pulsars could be determined by considering multi-wavelength observations (Pavlov et al., 1996). Since the measured spectra are however restricted to the X-ray energy band up to now, one is not in the position to determine the kind of atmosphere. For that reason we investigated both the black-body model and the hydrogen-atmosphere model, distinguished in Figs. 2 to 6 by error bars with a solid and hollow circle, respectively. All error bars represent the 2σ error range due to the small photon fluxes.

Except for PSRs 0833-45 (Vela) and 0002+62, all ages are estimated by their spin-down age $\tau = P/2\dot{P}$. This relation implies however that both the moment of inertia and the magnetic surface field are constant with time, and that the braking index n is equal to its canonical value 3 (angular momentum loss due to pure magnetic dipole radiation). The true ages may therefore be quite different from the spin-down ages. The age of Vela was recently

Table 3. Surface temperatures as measured by an observer at infinity, T_s^∞ , and spin-down ages, τ , of observed pulsars.

Pulsar	$\log \tau$ [yrs]	Model atmosphere	$\log T_s^\infty$ [K]	Reference
0002+62	$\sim 4 \dagger$	blackbody	$6.20^{+0.07}_{-0.27}$	Hailey & Craig (1995), Fig. 2 with lower limit on N_H
0833-45 (Vela)	$4.4 \pm 0.1 \dagger$	blackbody	6.24 ± 0.03	Ögelman (1995), Table III
		magnetic H-atmosphere	5.85 ± 0.09	Page et al. (1996), Fig. 1
0656+14	5.05	blackbody	$5.89^{+0.06 \ddagger}_{-0.17 \ddagger}$	Greiveldinger et al. (1996), Table 2
		magnetic H-atmosphere	$5.72^{+0.06 \ddagger}_{-0.05 \ddagger}$	Anderson et al. (1993)
0630+18 (Geminga)	5.53	blackbody	$5.75^{+0.05}_{-0.08}$	Halpern & Wang (1997), Table 2
		magnetic H-atmosphere	$5.42^{+0.12}_{-0.04}$	Meyer et al. (1994), Fig. 2a with $B_{12} = 1.18$
1055-52	5.73	blackbody	$5.90^{+0.06 \ddagger}_{-0.12 \ddagger}$	Greiveldinger et al. (1996), Table 2

\dagger estimated true age instead of spin-down age (see text).

\ddagger The 2σ range is not given in the respective reference. We therefore estimated it by multiplying the given 1σ error with a factor 2.

determined by Lyne et al. (1996), and the approximate age of PSR 0002+62 is given by an estimate of the age of the related supernova remnant G 117.7+06 (Hailey & Craig, 1995).

All calculations were performed for a gravitational mass of $M = 1.4M_\odot$, about which the observed pulsar masses tend to scatter. In Figs. 2 to 6, we plot the surface temperature of the neutron star models, as observed at infinity, against the stars age. Figure 2 shows the cooling bands for superfluidity case 1 and the equation of state classes A–D (see Sect. 4 for the definition of the classes). Superfluidity suppresses the nucleon processes so strongly, that the bands of the three classes standard, intermediate and enhanced nucleon cooling nearly coincide. Since the hyperon processes are not suppressed within the models used here, the band of scenario D1 is located much below the other three bands. Note that the relatively low surface temperature, in comparison with other works (e.g. Umeda et al., 1994; Page, 1995; Schaab et al., 1996), of the standard scenario A1 is caused by the inclusion of the superfluid pair breaking and formation process (Voskresenskii & Senatorov, 1987; Schaab et al., 1997), which is not included in older works. The surface temperature obtained by fitting with a magnetic hydrogen atmosphere (hollow circles) lie right between the scenario D1 and the scenarios A1–C1. In this model of superfluidity the gap between the bands can only be filled by reducing the superfluid critical temperature of the neutrons (Page, 1995; Schaab et al., 1996).

By increasing the inner magnetic field strength above its critical value we reach the second case of superfluidity (Fig. 3). Band C2, which corresponds to enhanced nucleon cooling, moves to lower temperatures. The observation of PSR 0630+18 (Geminga) is now consistent with this scenario as long as this pulsars has a magnetised hydrogen atmosphere.

If the magnetic field is in the order of the critical field strength but still below it, a $m = 2$ -superfluid is first formed by the neutrons, and later (as the star cools below

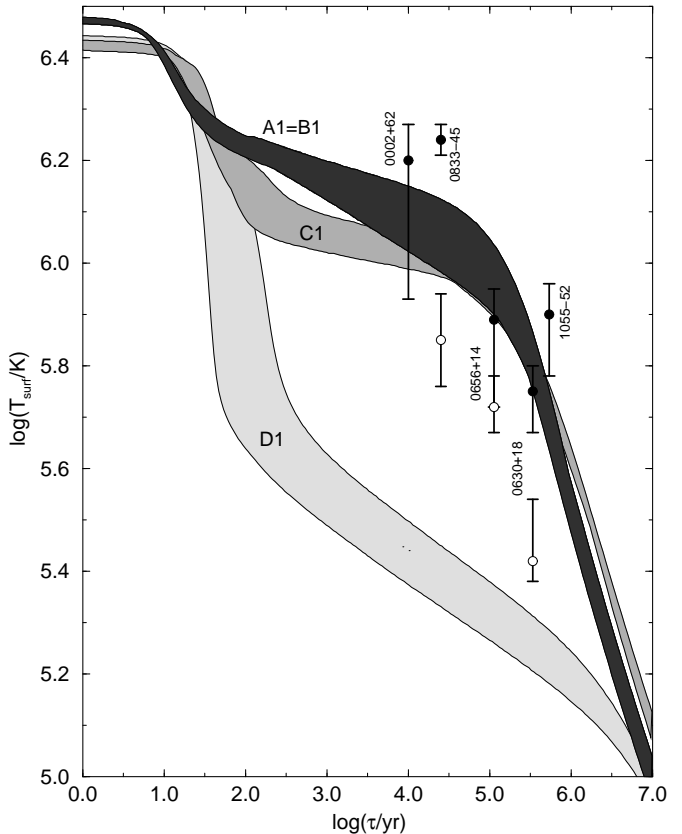


Fig. 2. Thermal evolution of a $M = 1.4M_\odot$ neutron star with superfluidity class 1. The bands correspond to the four classes of the equation of states as described in Sect. 4.

$T_{c,2}$, see Eq. 5) this superfluid turns into a nodeless state. This possibility is referred to by class 3 (Fig. 4). Only in scenarios C3 and D3 the temperature reaches this second critical value $T_{c,2}$ during the neutrino cooling era, that is during the time where cooling is dominated by energy loss due to neutrino emission. For that reason the band of the C3-scenario is pushed up again to higher temper-

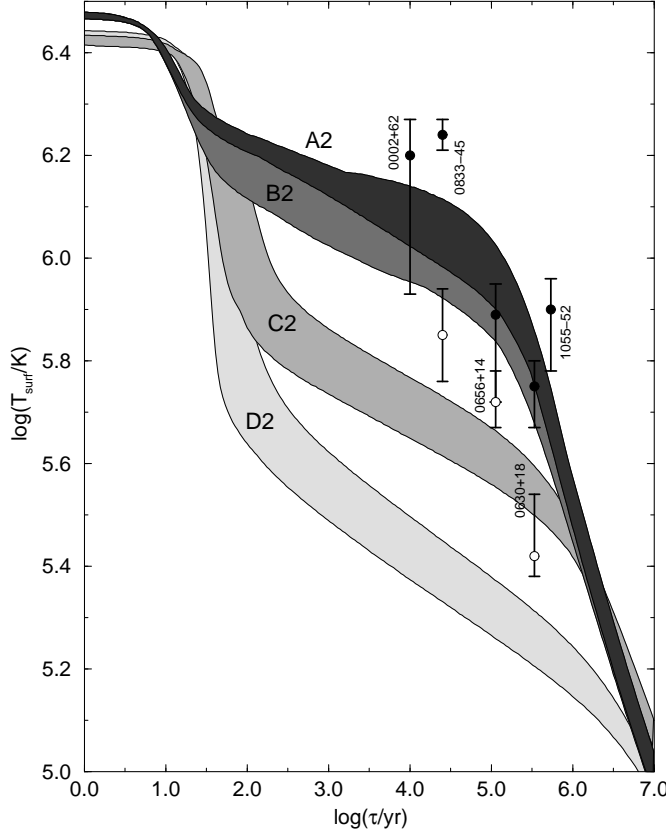


Fig. 3. Same as Fig. 2 but for superfluidity class 2.

ature which are consistent with the surface temperature obtained by fitting the observations with a magnetised hydrogen atmosphere (apart from PSR 0630+18). Scenarios B3 and A3 show again the same cooling behaviour.

In case 4, we assume that the neutron superfluid does not extend throughout the whole neutron star's core or the critical temperature is very small $T_c \lesssim 10^8$ K (Fig. 5). Then the nucleon processes are not suppressed everywhere, and particularly the models of the C4-scenario of enhanced nucleon cooling cool down very fast. Certainly this scenario, as well as scenarios D1–D4, is not consistent with the observations, no matter what kind of atmosphere is used. Case 4 would therefore clearly favour the standard or the intermediate cooling scenarios. The higher emissivity of the modified Urca process in scenario B4 lead now to considerably smaller surface temperatures in comparison with scenario A4.

Finally we consider the case 2γ , where the critical field strength $H_c(T = 0)$ is exceeded only inside the flux tubes. The suppression factor \mathcal{R} in Eq. (17) depends on the volume fraction γ occupied by the flux tubes. We study the cooling behaviour for two values of γ : $\gamma = 10^{-4}$, which corresponds to a bulk magnetic field strength $H = 2 \times 10^{13}$ G (see Eq. 18), and $\gamma = 10^{-2}$, which corresponds to $H = 2 \times 10^{15}$ G. To clarify the impact of this case on the cooling history of neutron stars, we plot cooling tracks for the

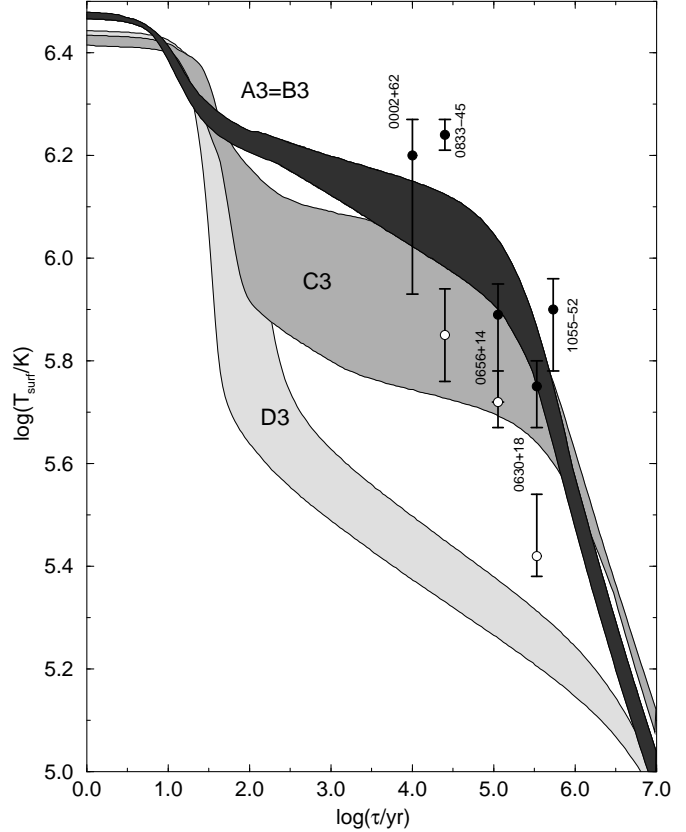


Fig. 4. Same as Fig. 2 but for superfluidity class 3.

HV_{pn} equation of state instead of bands (Fig. 6). Since the neutrino emission is exponentially suppressed only outside the proton flux tubes the effect of suppression is not as high as in the case of model C1 (which corresponds to $\gamma = 0$), but still larger than in the model C2 (which corresponds to $\gamma = 1$). The obtained surface temperatures are consistent with the surface temperature obtained by fitting the observations with a magnetic hydrogen atmosphere (again apart from PSR 0656+14). Although the surface temperature obtained in both scenarios C3 and C2 γ with $\gamma = 10^{-2}$ are consistent with the observation of PSR 0656+14 within the magnetic hydrogen atmosphere model, the bulk magnetic field strength in both models differ by two orders of magnitude.

6. Conclusions and discussion

In this work we have incorporated the possibility of nodes of the neutron gap energy along the magnetic axis in the core of a neutron star in simulations of thermal evolution. The realization of such superfluids depends on a rather strong magnetic field, that might however occur in the interior of a neutron star or in the interior of flux tubes of the proton type II superconductor. In any case the state of $m = 2$ -superfluid turned out to have several interesting consequences.

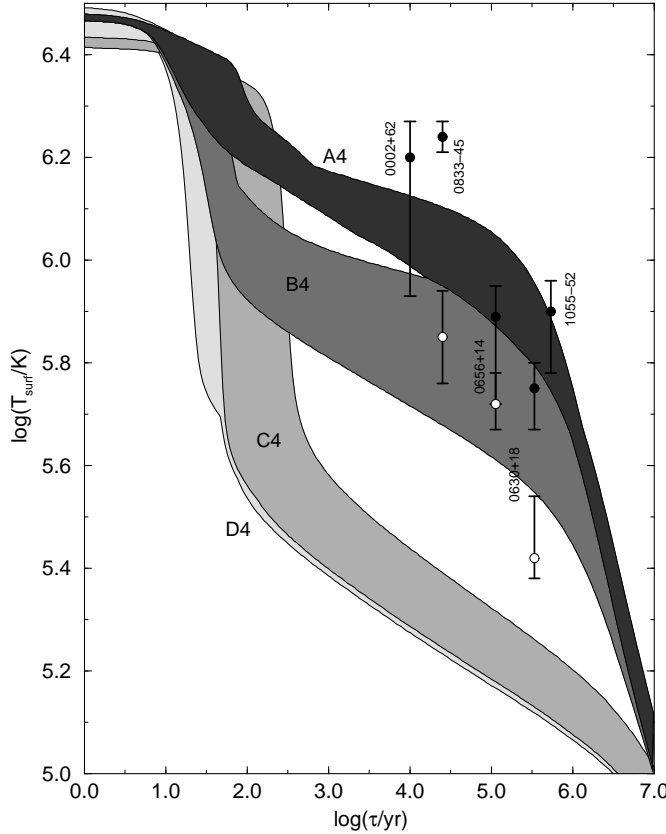


Fig. 5. Same as Fig. 2 but for superfluidity class 4.

Since the suppression factor \mathcal{R} of neutrino emissivity decreases only polynomially as function of T/T_c instead of exponentially, the effect of superfluidity is not as large as in the case of nodeless ($m = 0$) neutron superfluidity, which was studied in literature so far. Particularly the differences in the undiminished neutrino emissivities of the cooling classes A–D remain visible in the resulting surface temperatures.

The second important consequence is that in scenario C3 the second critical temperature $T_{c,2}$ depends on the internal magnetic field (see, Eq. 5). In scenario C2 γ the suppression factor depends on the factor γ (see Eq. 17), which itself depends on the bulk magnetic field strength (see Eq. 18). By varying the magnetic field the band corresponding to scenarios C2 γ and C3 can be moved to lower or higher surface temperatures in the age-range $10^2 \text{ yr} \lesssim \tau \lesssim 10^5 \text{ yr}$. This can also be achieved by varying the maximum energy gap, as it was done by Page (1995) and Schaab et al. (1996). Provided, that the energy gap reaches its maximum value for densities smaller than the central density of a typical neutron star, the maximum energy gap should be the same for all neutron stars. This is different with respect to the inner magnetic field strength since at least the surface magnetic field strengths of individual pulsars differ by five orders of magnitudes. This consequence may become important if two neutron stars are found which

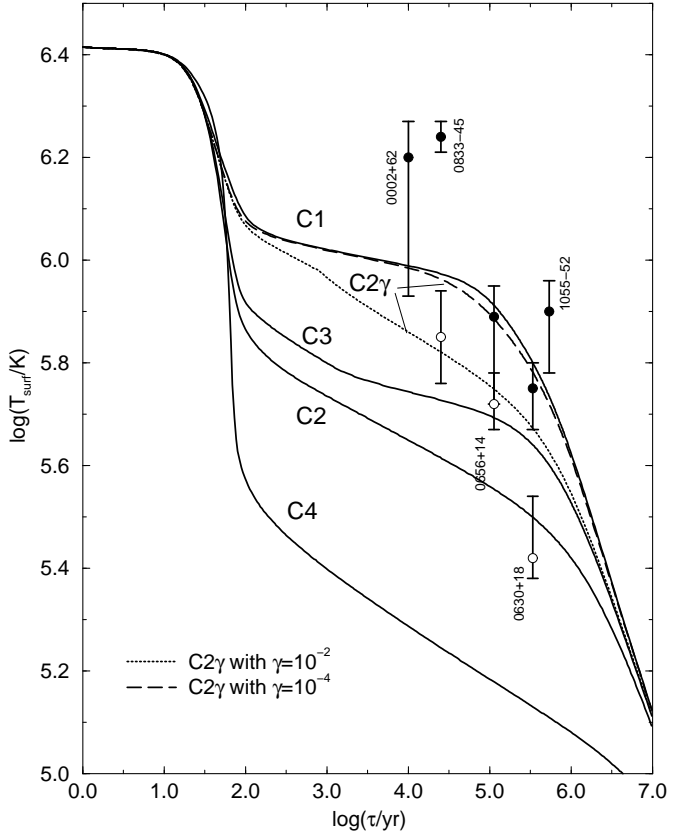


Fig. 6. Thermal evolution of a $M = 1.4M_{\odot}$ neutron star obtained for the HV_{pn} equation of state. The curves correspond to different superfluidity classes.

have about the same age but different surface temperatures, thought this might also be explained by different star masses in connection with the intermediate cooling scenario (see Fig. 8 in Schaab et al., 1997) and by more or less accreted matter on the surface of the star (see Fig. 9 in Potekhin et al., 1997). The two scenarios C2 γ and C3 differ in the internal magnetic field strength which is needed to explain, e.g., the surface temperature of PSR 0656+14 obtained within the hydrogen atmosphere model. Whereas for scenario C3 the rather strong magnetic field $H \sim 10^{17} \text{ G}$ is needed, a bulk magnetic field strength $H \sim 10^{15} \text{ G}$ is sufficient in scenario C2 γ .

The possibility of the direct nucleon Urca process becomes more and more probable. To the best of our knowledge all relativistic Hartree-, Hartree-Fock-, and Brückner-Hartree-Fock-equations of state have sufficiently large proton fractions to allow for the direct Urca process. In the past there were some doubt about the reliability of such high proton fractions, because the nonrelativistic variational equations of state, like UV₁₄+UVII and UV₁₄+TNI (Wiringa et al., 1988), predict proton fractions which are below the threshold value for the direct Urca process, since the symmetry energy does not monotonously increase with density. This seems to depend

however on the used potentials, since more modern potentials, like AV₁₈, Nijm-I,II, Reid93 and CD-Bonn, yield higher proton fractions (Engvik et al., 1997).

It seems therefore reasonable to restrict our following discussion to classes C and D. Since the impact of hyperon pairing has not been investigated yet, let us assume that all observed neutron stars belong to class C. Under this assumption the situation would become rather enlightened if the chemical composition of the neutron stars envelope could be determined by multi-wavelength observations. In the case that the blackbody fits will turn out to be adequate only scenario C1 is in agreement with the observations. If the magnetic hydrogen fits are more reasonable only scenarios C2, C2 γ , and C3 are consistent with the data. However also scenarios C1 and C4 can be brought into agreement if one reduces the gap energy in the case of C1 (Page, 1995; Schaab et al., 1996) or takes effects of an accreted envelope into account in the case of C4 (Potekhin et al., 1997; Page, 1996). As it was already claimed, these different scenarios could be further distinguished, if the surface temperature of two or more neutron stars with similar ages could be determined.

Acknowledgements. We like to thank the referee for his valuable comments. One of us (Ch. S.) gratefully acknowledges the Bavarian State for financial support. Tables with detailed references to the used ingredients and with the obtained cooling tracks can be found on the Web: <http://www.physik.uni-muenchen.de/sektion/suessmann/astro/cool/schaab.0797>.

References

Amundsen L., Østgaard E., 1985, Nucl. Phys. A 442, 163
 Anderson P.W., Morel P., 1961, Phys. Rev. 123, 1911
 Anderson S.B., Cordova F.A., Pavlov G.G., Robinson C.R., R. J. Thompson j., 1993, ApJ 414, 867
 Balberg S., Barnea N., 1998, Phys. Rev. C 57, 409
 Bisnovatyi-Kogan G.S., 1993, Astron. Astrophys. Trans. 3, 287
 Bisnovatyi-Kogan G.S., Moschenko I., 1992, SvA 36, 285
 Boguta J., 1981, Phys. Rev. Lett. 106B, 255
 Duncan R.C., Thompson C., 1992, ApJ 392, L9
 Elgarøy Ø., Engvik L., Hjorth-Jensen M., Osnes E., 1996a, Phys. Rev. Lett. 77, 1428
 Elgarøy Ø., Engvik L., Hjorth-Jensen M., Osnes E., 1996b, Nucl. Phys. A 607, 425
 Engvik L., Hjorth-Jensen M., Machleidt R., Muther H., Polls A., 1997, Nucl. Phys. A 627, 85
 Friman B.L., Maxwell O.V., 1979, ApJ 232, 541
 Gnedin O.Y., Yakovlev D., 1995, Nucl. Phys. A 582, 697
 Greiveldinger C., Camerini U., Fry W., et al., 1996, ApJ 465, L35
 Haensel P., Kaminker A.D., Yakovlev D.G., 1996, A&A 314, 328
 Hailey C.J., Craig W.W., 1995, ApJ 455, L151
 Halpern J.P., Wang F.Y.H., 1997, ApJ 477, 905
 Hoffberg M., Glassgold A.E., Richardson R.W., Ruderman M., 1970, Phys. Rev. Lett. 24, 775
 Huber H., Weber F., Weigel M.K., Schaab C., 1997, Neutron star properties with relativistic equations of state, to be published in Int. J. of Mod. Phys. E, preprint nucl-th/9711025
 Itoh N., Tomoo A., Nakagawa M., Kohyama Y., 1989, ApJ 339, 354
 Kaminker A.D., Yakovlev D.G., Haensel P., 1997, A&A 325, 391
 Lai D., Shapiro S.L., 1991, ApJ 383, 745
 Lattimer J.M., Pethick C., Prakash M., Haensel P., 1991, Phys. Rev. Lett. 66, 2701
 Levenfish K.P., Yakovlev D.G., 1994a, Astronomy Reports 38, 247
 Levenfish K.P., Yakovlev D.G., 1994b, Pisma Astron. Zh. 20, 54
 Levenfish K.P., Yakovlev D.G., 1996, Astron. Lett. 22, 56
 Lifshitz E.M., Pitaevskii L.P., 1980, Statistical Physics, part 2, Pergamon, Oxford
 Lyne A.G., Pritchard R.S., Graham-Smith F., Camilo F., 1996, Nat 381, 497
 Meyer R., Parlov G., Mészáros P., 1994, ApJ 433, 265
 Muslimov A., Page D., 1996, ApJ 458, 347
 Muzikar P., Sauls J., Serene J., 1980, Phys. Rev. D 21, 1494
 Ögelman H., 1995, in Alpar M., Kiziloglu Ü., van Paradijs J. (eds.), The Lives of the Neutron Stars, Kluwer, Dordrecht, p. 101
 Page D., 1995, Revi. Mex. Fís. 41, Supl. 1, 178
 Page D., 1996, ApJ 479, L43
 Page D., Shibanov Y.A., Zavlin V.E., 1996, in Röntgenstrahlung from the Universe: International Conference on X-Ray Astronomy and Astrophysics. MPE Report 263, 103, Max-Planck-Inst. Extraterr. Phys., Garching
 Pavlov G., Zavlin V., Trümper J., Neuhäuser R., 1996, ApJ 472, L33
 Potekhin A.Y., Chabrier G., Yakovlev D.G., 1997, A&A 323, 413
 Prakash M., Prakash M., Lattimer J., Pethick C., 1992, ApJ 390, L77
 Schaab C., Weber F., Weigel M.K., Glendenning N.K., 1996, Nucl. Phys. A 605, 531
 Schaab C., Voskresenskii D., Sedrakian A.D., Weber F., Weigel M.K., 1997, A&A 321, 591
 Schaab C., Balberg S., Schaffner-Bielich J., 1998, Implications of Hyperon Pairing for Cooling of Neutron Stars, subm. to ApJL
 Strobel K., Weber F., Weigel M.K., Schaab C., 1997, Int. J. of Mod. Phys. E 6, 669
 Takatsuka T., 1972, Prog. Theor. Phys. 48, 1517
 Taylor J.H., Manchester R.N., Lyne A.G., 1993, ApJS 88, 529
 Thompson C., Duncan R.C., 1993, ApJ 408, 194
 Thorne K., 1977, ApJ 212, 825

Umeda H., Tsuruta S., Nomoto K., 1994, ApJ 433, 256
Voskresenskii D.N., Senatorov A.V., 1986, Zh. Eksp. Teor. Fiz. 90, 1505
Voskresenskii D.N., Senatorov A.V., 1987, Sov. J. Nucl. Phys. 45, 411
Weber F., Weigel M., 1989, Nucl. Phys. A 505, 779
Wiringa R., Fiks V., Fabrocini A., 1988, Phys. Rev. C 38, 1010
Yakovlev D., Kaminker A., 1996, Astron. Lett. 22, 491
Yakovlev D.G., Levenfish K.P., 1995, A & A 297, 717